A Practical Solution for the Current and Voltage Fluctuation in Power Systems

A. Elnady and Yan-Fei Liu, *Senior Member, IEEE*

Abstract—This paper presents an innovative formulation and implementation for the steepest descent method to minimize the current and voltage fluctuation in power systems. The steepest decent is selected because of its mathematical simplicity. Its main disadvantage is circumvented by proposing a technique that selects proper initial values in order to guarantee its convergence. This technique depends on the Yule–Walker equation. The suggested technique for disturbance extraction is utilized to operate a power conditioner in order to mitigate the current fluctuation, and its performance is compared with the output of the vector control that is commonly used for the mitigation of the current and voltage fluctuation. The presented ideas are conveyed and approved through simulation results using Malab/Simulink. Moreover, some experimental results are provided to affirm the practicality of the presented concepts.

Index Terms—Steepest decent method, vector control and fluctuation compensation.

I. INTRODUCTION

FLUCTUATION in voltage and current is a common problem in the industrial distribution systems because of the proliferation of the nonlinear loads, such as arc furnaces, arc welders, spot welders, resistance welders, and repetitive operation of machinery. The nonlinear load draws a variable current from the source, which causes a variable voltage drop and voltage fluctuation at the point of common coupling (PCC). The arc furnace is the most common and dangerous source for the current fluctuation and voltage flicker in the industrial distribution systems [1].

The operation of the ac arc furnace consists of two major processes: 1) the melting process and 2) the refining process. The current fluctuation of the arc furnace is influenced by some factors, such as the melting or refining materials; the melting stage; the electrode position; the stiffness of the system; the short-circuit capacity; the furnace ratings; the supply system voltage; and its impedance, including its X/R ratio [2], [3]. The real spectrum of the generated voltage harmonics from the ac arc furnace reveals characteristic and noncharacteristic harmonics in addition to voltage unbalance [2], [4]–[6]. Also, some other studies prove that the real harmonic spectrum of the arc furnaces contains some subharmonics and interharmonics as well [7], [8].

The common mitigation devices for the fluctuation are the distribution static compensator (DSTATCOM) in the distribution systems [9] and STATCOM in the transmission systems [10], [11]. These mitigation devices are commonly operated by the d–q vector control, which includes two loops. The first loop controls the direct current or voltage to stabilize the dc side of the mitigation device while the second loop adjusts the quadrature output current to compensate for the reactive current taken by the nonlinear loads [12], [13]. The d–q vector control has some shortcomings especially when this control strategy is used to compensate for the current fluctuation and voltage flicker of the arc furnaces. Thus, the d–q vector control does not provide excellent results, but it usually gives satisfactory results in the arc furnace environment [14].

The research in this paper is motivated by the pitfalls of the vector control in order to achieve better compensation for the current and voltage fluctuation. Therefore, the contribution of this paper is the innovative development of the steepest decent method to track the frequency, magnitude, and phase for the dominant components of the current disturbance resulting from the arc furnace; regardless of how these components are closely spaced in the frequency domain. Furthermore, the major drawback of the steepest decent, which is the selection of the initial values [15], is overcome by adopting another spectral estimation technique. This spectral technique depends on the Yule–Walker equation [16] to properly select the initial values that guarantee the convergence and accuracy of the steepest decent. The proposed techniques for disturbance tracking have the merit of the mathematical simplicity compared to the other techniques used for the same applications, such as the Kalman filter [17], [18] and ESPRIT [19], which are used to simultaneously estimate and track the frequency, magnitude, and phase of different sinusoids. This mathematical simplicity helps the proposed technique to perform instantaneous extraction and fast online tracking for the current disturbances.

This paper consists of seven sections. Section II shows the mathematical formulation of the proposed technique for the extraction of the current disturbance. Testing the proposed technique is documented in Section III. Section IV depicts the simulation results for flicker compensation compared with the results of the vector control for the same flicker disturbance. Section V exhibits the experimental results for the proposed concepts. Finally, the last two sections summarize the findings of this paper and the appendices.

A. Elnady is with the Electrical and Computer Engineering Department, University of Sharjah, Sharjah 27272, United Arab Emirates. He is also with RMC, Kingston, ON K7K 7B4, Canada (e-mail: ayelnady@hivolt.uwaterloo.ca).

Y. Liu is with the Department of Electrical and Computer Engineering, Queen's University, Kingston, ON K7L 3N6, Canada (e-mail: yanfie.liu@queensu.ca).

II. FORMULATION OF THE STEEPEST DECENT METHOD FOR DISTURBANCE EXTRACTION

The steepest decent is a very simple technique to find the minimum mean square error [15]. The distorted current can be expressed as

$$y(t) = \sum_{i=1}^{M} A_i \, \sin(\omega_i t + \phi_i) + s(t) \tag{1}$$

where A is the magnitude, ω is the angular frequency, ϕ is the phase, t is a particular sampling instant, M is a number of the components of interest for estimation, and s is the noise. The noise is neglected in this analysis because its value is small compared to y. The expected error is calculated as

$$e(t) = y(t) - \hat{I}(t) \tag{2}$$

where $\hat{}$ denotes an estimated value, and the estimated signal is expressed as

$$\hat{I}(t) = \sum_{i=1}^{M} \hat{A}_i \, \sin(\hat{\omega}_i t + \hat{\phi}_i). \tag{3}$$

The state variables that will be estimated are given as

$$x = [A_1 \, \omega_1 \, \varphi_1 \, A_2 \, \omega_2 \, \varphi_2 \, \ldots \, A_{M-1} \, \omega_{M-1} \, \varphi_{M-1} \, A_M \, \omega_M \, \varphi_M]. \tag{4}$$

To estimate vector x, the mean square error should be minimized, and its expression is written as

$$F = \sum_{t=1}^{N} e^2(t) \tag{5}$$

where N is the number of samples in the data set. The iterative formula for the steepest decent is given in [15] as

$$x(t+1) = x(t) - \alpha \nabla F_x \tag{6}$$

where x is the state vector as indicated in (4), α is a scalar value to control the step size, and ∇ indicates the gradient of F on the mean square error surface with respect to the vector x. The last term of (6) can be simplified using the Widrow–Hoff delta rule [20]; consequently, the iterative formula of (6) is rewritten as

$$x(t+1)_{[3M \times 1]} = x(t)_{[3M \times 1]} - \alpha \times e(t)_{[1]}$$
$$\times \frac{\sum_{t=1}^{N} \left[\frac{\partial e(t)}{\partial x} \right]_{[3M \times 1]}}{\sum_{t=1}^{N} \left[\frac{\partial e(t)}{\partial x} \right]_{[1 \times 3M]}^{T} \times \sum_{t=1}^{N} \left[\frac{\partial e(t)}{\partial x} \right]_{[3M \times 1]}} \tag{7}$$

where

$$\sum_{t=1}^{N} \left[\frac{\partial e(t)}{\partial x} \right] = \sum_{t=1}^{N} \begin{bmatrix} -\sin(\omega_1 t + \varphi_1) \\ -tA_1 \cos(\omega_1 t + \varphi_1) \\ -A_1 \cos(\omega_1 t + \varphi_1) \\ \vdots \\ -\sin(\omega_M t + \varphi_M) \\ -tA_M \cos(\omega_M t + \varphi_M) \\ -A_M \cos(\omega_M t + \varphi_M) \end{bmatrix}. \tag{8}$$

The iterative formula is efficiently utilized to track the sinusoids' parameters, but still the major pitfall of the steepest decent method exists, which is the selection of the initial values for the vector x. To guarantee the convergence of the steepest decent, the initial values should be localized close to the trough of the global minimum. Therefore, the initial values are estimated by utilizing the overdetermined Yule–Walker equation [16], [21]. It is intentionally selected because its covariance matrix is not affected by the presence of the white noise in addition to its mathematical simplicity.

For the autoregressive (AR) model of a finite set of data, the correlation coefficient R is defined as [16]

$$R_p = \frac{1}{N-p} \sum_{t=1}^{N-p} y(t) * y(t+p) \tag{9}$$

where p represents twice the number of components in signal y. The difference equation of the AR model can be rewritten using the Yule–Walker equation as

$$\sum_{k=1}^{p} a_k R_{m-k} = -R_m \rightarrow m = p+1, \ldots, 2p. \tag{10}$$

Formula (10) can be split into p equations in a_k coefficients, where $k = 1, 2, \ldots, p$. The matrix form of these equations can be expressed as

$$\begin{bmatrix} R_p & R_{p-1} & \ldots & R_1 \\ R_{p+1} & R_p & \ldots & R_2 \\ \vdots & & & \\ R_{2p-1} & R_{2p-2} & \ldots & R_P \end{bmatrix} \begin{bmatrix} a_1 \\ a_2 \\ \vdots \\ a_p \end{bmatrix} = \begin{bmatrix} -R_{p+1} \\ -R_{p+2} \\ \vdots \\ -R_{2p} \end{bmatrix} \tag{11}$$

or

$$[a]_{p \times 1} = [R]_{p \times p}^{-1} [-R']_{p \times 1}. \tag{12}$$

By solving (12), the a-vector can be obtained. Consequently, the corresponding, (maximum entropy), estimation of the input spectrum can be calculated from the zeros (roots) of the following characteristic polynomial:

$$H(z) = 1 + \sum_{k=1}^{p} a_k z^{-k} \tag{13}$$

where $z = e^{j\omega}$.

The estimated frequency can be obtained from the corresponding roots of the previous formula as

$$f_{\text{estimated}} = \frac{\cos^{-1}(\text{real}(\text{zeros of (13)}))}{2\pi} * f_{\text{sampling}}. \tag{14}$$

The inverse of the matrix $R_{p \times p}$ may impose a problem if the matrix is ill-conditioned. This case may arise when all of the initial magnitudes and frequencies are equal or are very close to each other. This problem is the only limitation for this technique, and it can be circumvented by a proper selection for initial magnitudes and frequencies in order to avoid the singularity in the matrix $R_{p \times p}$. This utilized technique for estimating the initial values can be applied only once at the beginning of operation for the proposed technique because any variation in the frequency can be automatically detected during the iterative operation of the steepest decent method.

III. EVALUATION FOR THE PROPOSED TECHNIQUES

In this section, the proposed formulation of the steepest decent and the Yule–Walker equation for estimating the initial values are tested to prove that they perform well for accurate tracking of the current disturbances. As mentioned before, the extended Kalman filter has been used for the same application [18]. This extended Kalman filter encompasses heavy mathematics and matrices operations, which hinder its practical implementation. Another technique, called ESPIRIT [19], has been utilized for the same application. Its operation depends on the application of a subspace estimation technique on a sliding window of many cycles, but it still suffers from the mathematical complexity and bad transient performance, which precludes its online disturbance extraction. The proposed technique cannot be compared with the Kalman filter and ESPIRIT because the proposed technique is much simpler than these techniques [17]–[19]. The possible candidate for a fair comparison is the adaptive notch filter that has been utilized for frequency detection [22] and for signal estimation [23]. The formulation of the adaptive notch filter to track the signal components, based on [24], is developed and listed in Appendix A. The test signal for performance evaluation is expressed in (15), where it is an example of the primary current for the arc furnace since it has some interharmonics and subharmonics [25]

$$
\begin{aligned}
I_{\text{fluctuation}} = {} & 43\sin(2\pi 22t + 0.2) \\
& + 46\sin(2\pi 37t + 0.1) \\
& + 16\sin(2\pi 45t + 0.4) \\
& + 785\sin(2\pi 50t + 0.3) \\
& + 35\sin(2\pi 65t + 0.66) \\
& + 56\sin(2\pi 72t + 0.27) \\
& + 30\sin(2\pi 80t + 0.22) \\
& + 11\sin(2\pi 141t + 0.4) \\
& + 11\sin(2\pi 155t + 0.4) \\
& + 9\sin(2\pi 202t + 0.2).
\end{aligned}
\tag{15}
$$

The developed formulation for the steepest decent is first examined without using any technique for estimating the initial values, which are randomly selected. The presented formulation of Section II, (the formula in (7)) is applied on the current of (15). The estimated frequencies are obtained as

$$
f_{\text{estimated}}(Hz) =
\begin{bmatrix}
21.978 \\
37.011 \\
16506 \\
50.026 \\
64.864 \\
71.794 \\
123.52 \\
173.9 \\
208.33 \\
202
\end{bmatrix}.
\tag{16}
$$

The previous estimated vector indicates that there is no accurate estimation for the 3rd, 7th, 8th, and 9th components of (15). The full tracking for magnitudes and phases associated with the
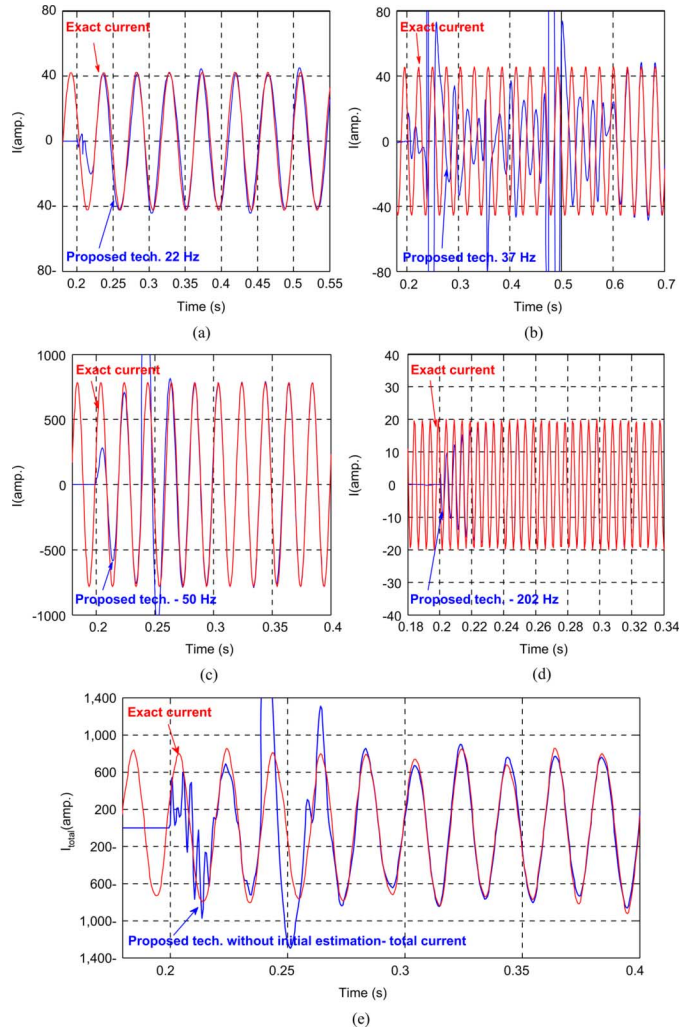

Fig. 1. Performance of the proposed technique without using the Yule–Walker equation for estimating the initial values. (a) Tracking of the 22-Hz component. (b) Tracking of the 37-Hz component. (c) Tracking of the 50-Hz component. (d) Tracking of the 202-Hz component. (e) Tracking for the total current of (15) by the proposed technique.

estimated frequencies is shown in Fig. 1, where just four components are shown in addition to the tracking for the total current of (15). The performance of Fig. 1 reveals the importance of utilizing the Yule–Walker equation for estimating the initial values. If there is no good estimate for the initial values, this may lead to inaccurate frequency estimation and inefficient tracking for that current disturbance. This inaccurate tracking performance is clearly depicted in Fig. 1(e).

In the following part, the proposed technique is accompanied by the utilization of the Yule–Walker equation for the estimation of the initial values. The results of the proposed techniques are compared with the adaptive notch filter as shown in Fig. 2 in which just four components are shown in addition to the tracking for the total current of (15).

The performance of the proposed techniques for tracking the current of (15) is depicted in Fig. 2, where each graph shows the performance of the proposed technique and the adaptive notch filter with respect to the exact signal. These waveforms confirm that the proposed technique is more accurate and faster
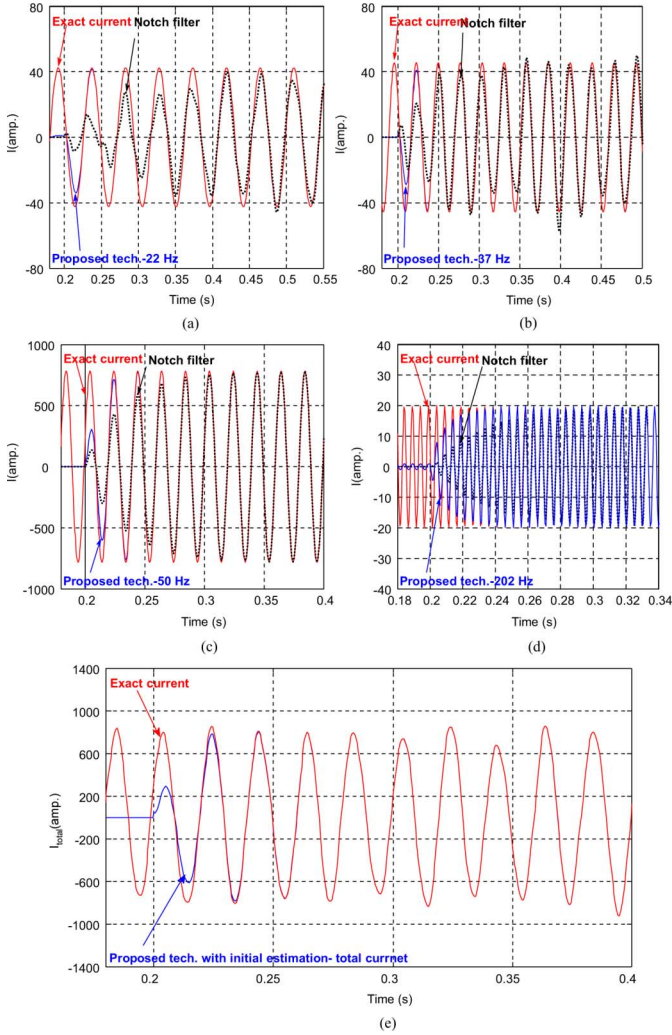
Fig. 2. Comparison between the proposed technique associated with the Yule–Walker equation and adaptive notch filter for the tracking current fluctuation of (15). (a) Tracking of the 22-Hz component. (b) Tracking of the 37-Hz component. (c) Tracking of the 50-Hz component. (d) Tracking of the 202-Hz component. (e) Tracking for a total current of (15) by the proposed techniques.

than the adaptive notch filter for signal tracking. Furthermore, the proposed technique has better dynamic performance since it reaches its steady state within almost two cycles. This point is clearly shown in Fig. 2(e).

IV. SIMULATION RESULTS

This section displays the simulation results for the mitigation of the current and voltage fluctuation using the proposed techniques. These results are compared with the results of the d–q vector control for the DSTATCOM. This section includes two subsections: the first subsection illustrates the simulation results of the proposed techniques for the compensation of the current and voltage fluctuation. The second subsection depicts the simulation results for the current vector control of the DSTATCOM for the same disturbance. The system under study, shown in Fig. 3, is part of a real distribution system in the U.S. [4].
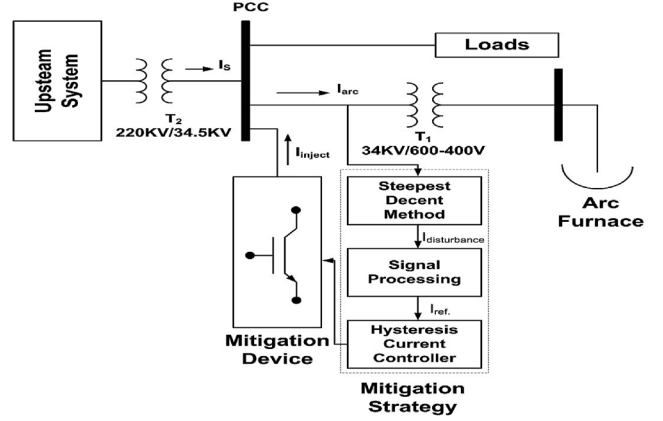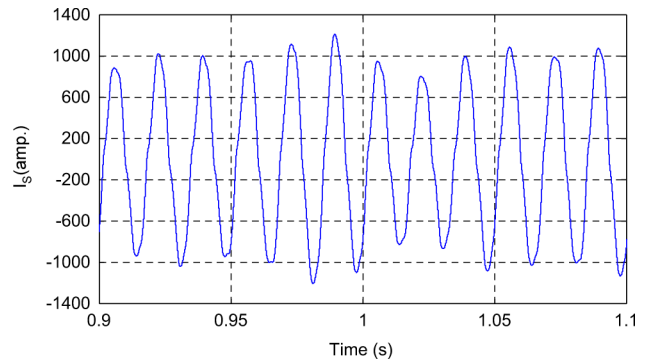

Fig. 3. System under study.

Fig. 4. Current fluctuation due to the operation of the arc furnace.

A. Mitigation Results by the Proposed Technique

The system under study is simulated using Matlab/Simulink, and the proposed mitigation strategy is integrated in this system of Fig. 3. The details of the arc furnace model and simulation parameters are given in Appendices B and C, respectively. This mitigation strategy consists of the proposed technique for disturbance extraction, which yields a reference current that is processed by the hysteresis current controller to operate a mitigation device, (power conditioner). This power conditioner injects a current that stabilizes the current and voltage at the upstream system. The mitigation device of Fig. 3 is a single-phase voltage-source converter, and each single-phase circuit has a dedicated single-phase mitigation device. The arc furnace is modeled and embedded in the system under study. The adopted model for the arc furnace is the current-controlled nonlinear time-domain model mentioned in [26]. The outcome of this accurate arc furnace model gives I_s that is illustrated in Fig. 4.

The current waveform of Fig. 4 is applied to the proposed formulation of Section II. The proposed techniques give the estimated frequencies and different current components. Fig. 5(a) shows the estimated frequencies of the ten dominant components. The error percentage between the total estimated components and the exact current waveform in Fig. 4 is illustrated in Fig. 5(b). It is obvious that this error percentage never exceeds 5%, which is good for the frequency, magnitude, and phase estimation for about ten different components. Also, Fig. 5(c)-(f) illustrates just the four dominant components at frequencies 36,
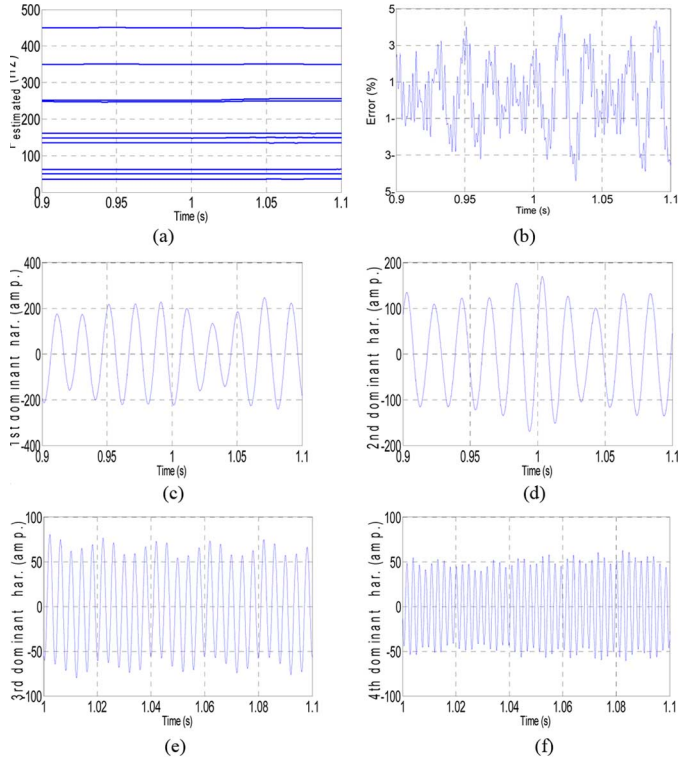
Fig. 5. Performance of tracking for the current of Fig. 4. (a) Estimation of the dominant ten frequencies for the current in Fig. 4. (b) Error percent between the total extracted disturbance and the current of Fig. 4. (c) Tracking of the 1st dominant harmonic current with 36 Hz. (d) Tracking of the 2nd dominant harmonic current with 63 Hz. (e) Tracking of the 3rd dominant harmonic current with 250 Hz. (f) Tracking of the 4th dominant harmonic current with 350 Hz.

63, 250, and 350 Hz. These curves [Fig. 5(c)–(f)] indicate that the magnitudes of the disturbance for the arc furnace are variable and that is why the current of Fig. 4 looks random in variation.

Another merit for the presented extraction technique is its ability to track the active and reactive components of the fundamental current, which can be obtained through the magnitude and angle of this component. Thus, the fundamental reactive component, taken by the furnace, can be easily extracted and included in the reference and compensated currents. Fig. 6 shows the total extracted disturbance and the fundamental reactive component. The extracted disturbance of Fig. 6(a) is the instantaneous sum for the dominant disturbance components of the current in Fig. 4 while Fig. 6(b) shows the reactive component of the fundamental current.

The mitigation for the current disturbance and the reactive fundamental component is demonstrated in Fig. 7, where this waveform represents the fundamental active current, which has a slight fluctuation because of the variable arc resistance of the arc furnace model. The justification for the current improvement is conveyed through the total harmonic distortion (THD) for I_s, which is 5.1% in Fig. 7. The reflection of this mitigation is manifested in the variation for the voltage at the PCC for the system shown in Fig. 3, in which there is a permanent voltage drop because of the current taken by the arc furnace. The voltage waveforms at PCC before and after the mitigation are illustrated in Figs. 8 and 9, respectively.
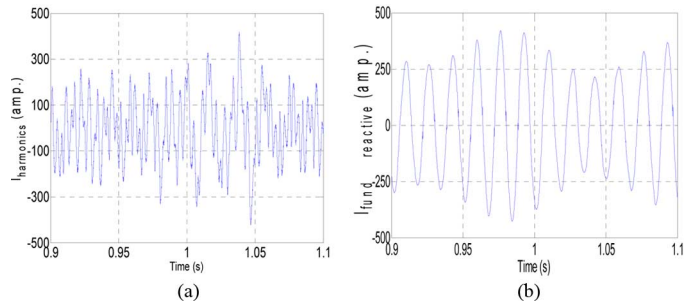
Fig. 6. Extracted disturbance signal and reactive fundamental. (a) Disturbance current. (all harmonics). (b) Fundamental reactive component taken by the arc furnace.
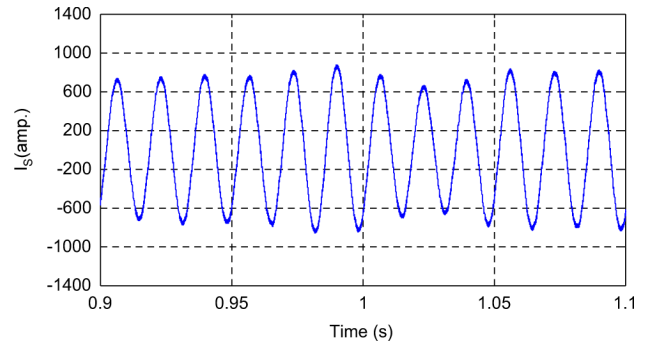
Fig. 7. Mitigation for the current shown in Fig. 4 by the proposed technique.
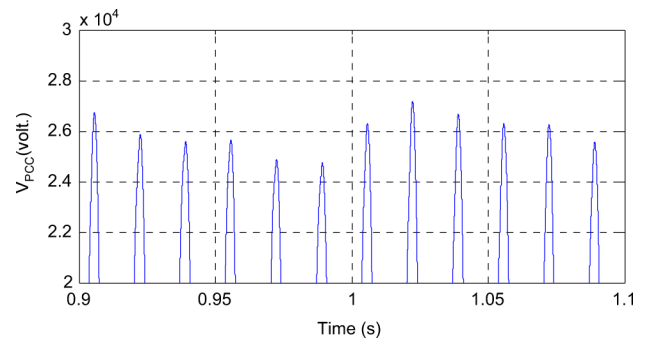
Fig. 8. Voltage profile because of the arc furnace operation.

Fig. 9. Voltage profile after compensation by the proposed technique.

The flicker can be quantified by a simple flicker factor that calculates the percent change in voltage $\Delta V/V_0$ as expressed in IEEE Standard 141. Thus, this flicker factor is reduced from

Fig. 10. Vector control block diagram for single-phase D-STATCOM.

Fig. 11. Performance for the two loops of Fig. 11. (a) DC voltage control. (b) Reactive power for arc furnace and DSTATCOM.

7.6% to 1.28%, which indicates that the flicker level is transferred from the objectionable region to the noticeable region based on IEEE Standard 141.

B. Mitigation Results by the d–q Vector Control Technique

The d–q vector control is commonly used to operate the DSTATCOM and STATCOM in order to mitigate the voltage and current fluctuation. The operation and the structure of its control block 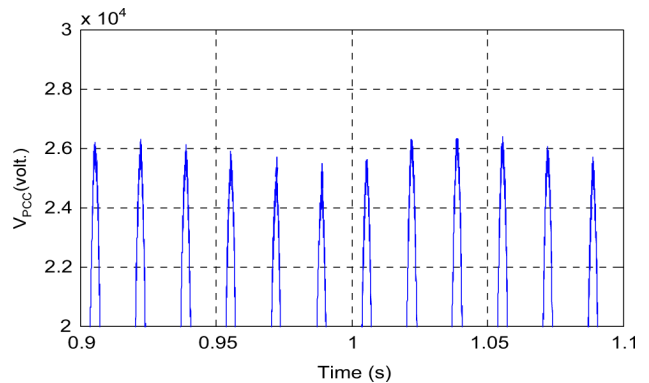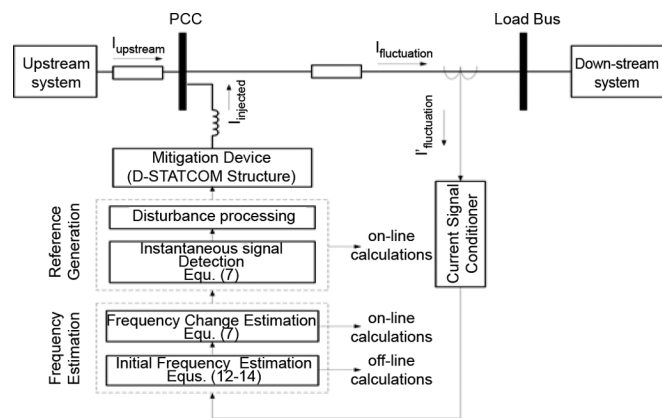diagram are well documented in [27]–[29]. This control technique gives convenient results, but it does not give excellent results in the arc furnace environment because the operation of the DSTATCOM is associated with some drawbacks in this environment [14]. To justify the good performance of the suggested mitigation strategy in the arc furnace environment, the performance of the d–q vector control is given for the same current and voltage fluctuation generated from the arc furnace of Fig. 3. The utilized block diagram of the d–q vector control is given in Fig. 10, in which two control loops are depicted; the first loop is designated to compensate for the reactive power consumed by the arc furnace, while the second the loop is used to stabilize the dc voltage value. The performance of this block diagram is shown in Fig. 11, where the Q-DSTATCOM tracks the Q-arc as in Fig. 11(b), and the V_{DC} of the DSTATCOM is nearly constant with a variation of 0.5% around its steady-state value as depicted in Fig. 11(a). This performance has an impact on the mitigation of the current fluctuation as shown in Fig. 12, which still indicates some sort of current fluctuation. This fluctuation comes from some harmonics and the fundamental active component taken by the arc furnace. Consequently, the current mitigation impacts the voltage flicker at the PCC. Its voltage waveform is portrayed in Fig. 13.

The comparison between Figs. 7 and 12 affirms the superior performance of the proposed techniques to the d–q current vector technique for the mitigation of the current fluctuation because the current of Fig. 7 indicates the fundamental component without influential harmonic distortion, but the current in Fig. 12 shows harmonic disturbances superimposed on the fluctuating fundamental component. The distortion of Fig. 12 results from the complexity of the control scheme [27], the delay associated with the PI controllers utilized in the vector control (depicted in Fig. 11(b) and in [12]), and the inability of the vector control to mitigate all of the interharmonics in the current fluctuation.

Fig. 12. Mitigated current by the d–q current vector control.

Fig. 13. Voltage profile after compensation by the d–q current vector control.

Therefore, the waveform of Fig. 12 is not a constant pure sinusoid, and it is clear from Fig. 12 that some harmonic distortion and fluctuation still exist. The mathematical justification for this meritorious performance is conveyed in the current THD after mitigation, which is 5.1% in Fig. 7 and 12.6% in Fig. 12. Also, the flicker factor, based on IEEE Standard 141, is 1.28% in Fig. 9 and 3.9% in Fig. 13.

V. PRACTICAL IMPLEMENTATION

This section exhibits the practical implementation for the disturbance extraction technique of Section II, and its implementation to mitigate the current fluctuation as demonstrated in Section III. This section is split into four parts—the first part demonstrates how the proposed compensation strategy can be practically implemented in power systems. The second part illustrates the mitigation of the cyclic current fluctuation. The

Fig. 14. Structure of the practical implementation for the current and voltage improvement in power systems.

Fig. 15. Experimental setup for fluctuation compensation.

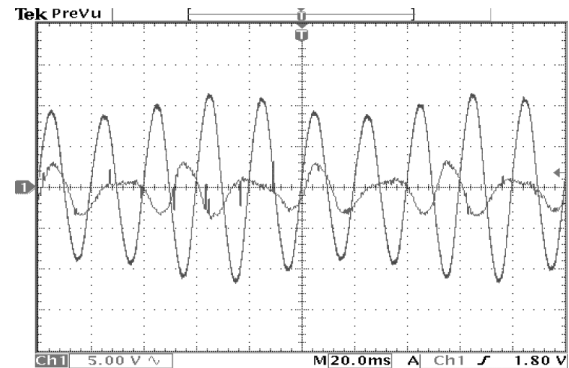

Fig. 16. Cyclic current fluctuation with a scale of 1 A/div and an extracted disturbance with a scale of 0.5 A/div.

third part shows the compensation of the irregular current fluctuation. The last part manifests the impact of current compensation on the voltage profile.

A. Structure of the Compensation Process in Power Systems

This part manifests how the proposed strategy is practically realized in power systems. The structure of the hardware setup is shown in Fig. 14, where it is not similar to the typical structure for the voltage-control scheme of the STATCOM or D-STATCOM [12]–[14], because the philosophy behind its operation for voltage control is different since the proposed strategy depends on the signal-processing techniques for generating the reference signals required to operate the mitigation device. The compensation process starts with sensing the distorted current, and the current conditioner adapts this distorted current to be ready for processing by a controller. This controller includes the digital signal processor and some other circuits responsible for generating the current reference and the hysteresis current controller. The preprocessing frequency estimation is done in the offline mode [(12)–(14)] to estimate the initial frequencies. Instantaneous signal detection (tracking for the frequency change, magnitude, and phase obtained from (7)) is recursively performed in the employed signal processor to generate the reference signal required for the current regulator of the mitigation device as demonstrated in Fig. 14.

The prototype setup includes a programmable ac voltage source, Chroma 61500, which is responsible for initiating the current fluctuation. The mitigation device is the IRF830 power metal–oxide semiconductor field-effect transistor (MOSFET)-based single-phase voltage-source converter operated by the hysteresis current controller. The disturbance extraction technique is programmed in eZdsp-LF2407A to generate the disturbance signal. The prototype circuit is given in Fig. 15. The important parameters for the experimental setup are listed in Appendix C.

B. Mitigation of the Cyclic Current Fluctuation

The cyclic current fluctuation is shown in Fig. 16, where the fundamental component is modulated by another sinusoidal

signal. This current fluctuation is applied to the proposed disturbance extraction technique, which is programmed on the employed digital signal processor, to track the current disturbance. This extracted disturbance is also demonstrated in Fig. 16. To justify the accuracy of the proposed technique for the disturbance extraction, the extracted disturbance and the exact disturbance, extracted by another analog filter, are illustrated in Fig. 17. In this figure, the extracted disturbance greatly matches the exact one. Finally, the compensation of the current fluctuation is given in Fig. 18, where the envelope of the peaks for the mitigated current waveform is almost constant compared to the similar envelope of the uncompensated current of Fig. 16.

C. Mitigation of the Nonuniform Current Fluctuation

The current fluctuation in this part is not cyclic because the fundamental component is modulated by some signals with different frequencies. This current fluctuation is displayed in Fig. 19, where the fluctuation looks more complicated than the previous case. The extracted disturbance by the proposed technique is also depicted in the same figure. The accuracy of the proposed technique can be proved through Fig. 20, since the extracted disturbance is almost similar to the exact disturbance. This extracted disturbance is employed to operate the hysteresis controller, and the power conditioner injects a certain current so that the total distortion can be minimized. Eventually, the compensation of the current fluctuation is illustrated in Fig. 21, which shows a drastic improvement for the envelope of the current fluctuation compared to the envelope of the current fluctuation in Fig. 19. Also, the improvement in the current quality is affirmed by calculating its THD, where its value is 6.2% in Fig. 21.
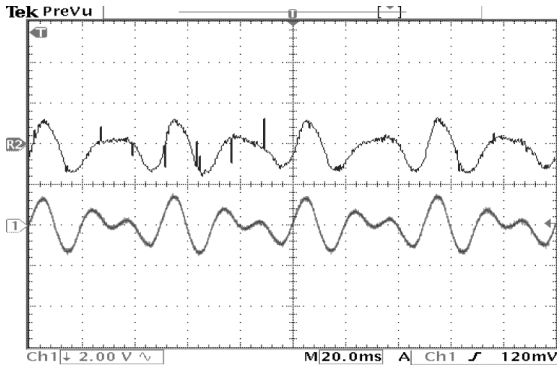
Fig. 17. Extracted disturbance signal with exact disturbance for the fluctuation of Fig. 15. The upper waveform indicates the extracted disturbance with a scale of 0.5 A/div, and the lower waveform represents the exact disturbance with a scale of 0.5 A/div.
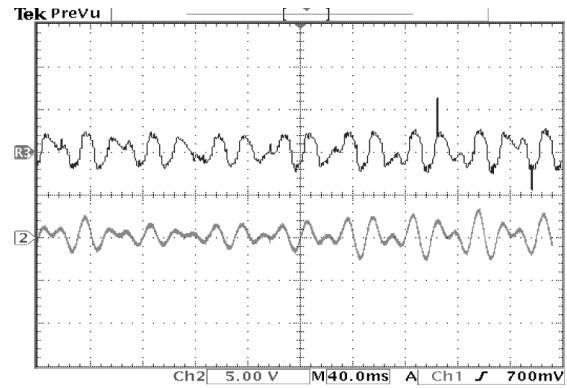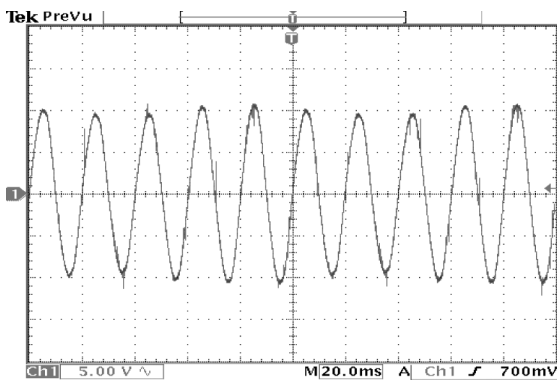

Fig. 20. Extracted disturbance signal with the exact disturbance. The upper waveform indicates the extracted disturbance with a scale of 1 A/div, the lower waveform represents the exact disturbance with a scale of 1 A/div.

Fig. 18. Compensation for the current fluctuation of Fig. 16 with a scale of 1 A/div.
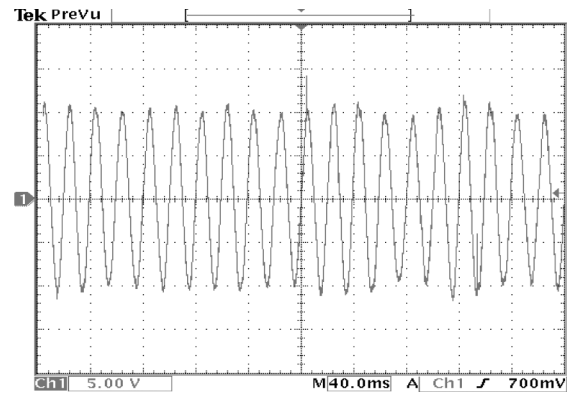
Fig. 21. Compensation for the current fluctuation of Fig. 18 with a scale of 1 A/div.
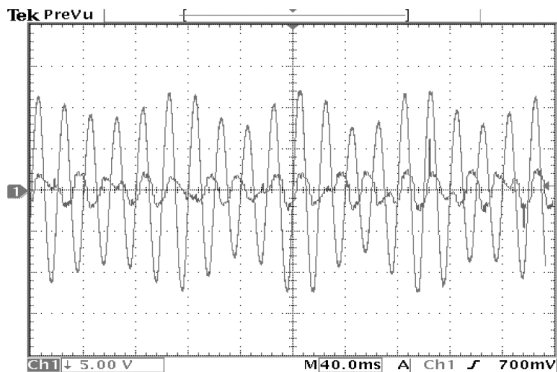
Fig. 19. Nonuniform current fluctuation with a scale of 1 A/div and extracted disturbance with a scale of 1 A/div.
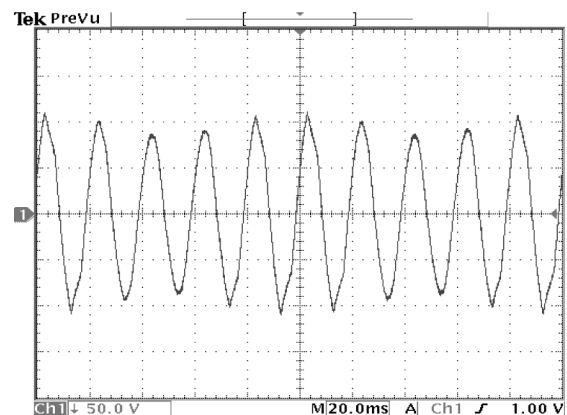

Fig. 22. Voltage flicker due to the current of Fig. 16 with a scale of 50 V/div.

D. Improvement of the Voltage Profile

Voltage flicker at the PCC results from the interaction between the fluctuating current and system impedance. Once the current fluctuation has been reduced, the voltage flicker is minimized correspondingly. The rated rms voltage value for the same prototype of Fig. 15 is 70 V.

The voltage flicker due to current fluctuation is depicted in Fig. 22, where the short-term severity factor P_{st} (obtained from the approximate form mentioned in [30]) is 2.27. The voltage waveform after the compensation for the current fluctuation is

illustrated in Fig. 23. The improvement of the voltage waveforms in Fig. 23 is confirmed through the value of its P_{st}, which is reduced to 0.91.

Finally, these experimental results are given to prove that the proposed compensation strategy achieves convenient results for the mitigation of the current fluctuation and voltage flicker. This meritorious performance is justified through:
1) the simple structure of the implemented compensation process as depicted in Fig. 14 compared to the structure of the vector control for the STATCOM [10], [12], [13];
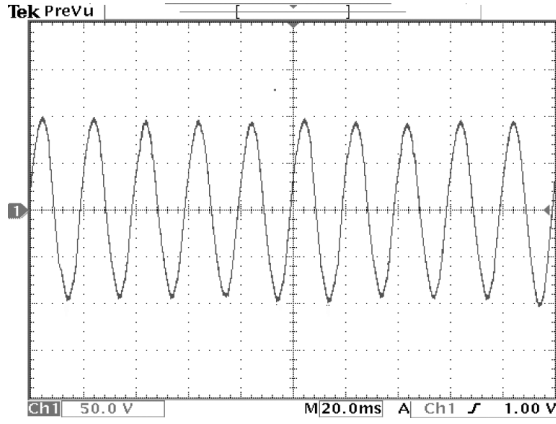
Fig. 23. Compensated voltage waveform for the flicker of Fig. 22 with a scale of 50 V/div.

2) the simple concept for mitigation, which implicates a direct injection for a certain current to minimize the current and voltage distortion generated by nonlinear loads, in addition to its capability for simple extraction and efficient compensation for the reactive components; whereas, this simple mitigation concept does not exist in the vector control scheme utilized for the operation of the STATCOM or DSTATCOM to mitigate the fluctuation of the arc furnace [12], [13].

VI. CONCLUSION

The derived formulas of the steepest decent method prove its ability to extract and track the disturbance components of the current fluctuation. Also, the utilization of the Yule–Walker equation improves the convergence of the developed technique, which guarantees the stability and reliability of the proposed extraction technique. The presented disturbance extraction technique performs well for the current fluctuation compared to the common techniques for the same applications. The experimental results of the developed technique affirm the practicality and its capability to compensate for the current fluctuation of nonlinear loads, such as arc furnaces.

APPENDIX A

Formulation of the adaptive notch filter.

The recursive adaptive notch is developed in this part. The transfer function of the notch filter is written as follows:

$$H(z) = \frac{e(k)}{x(k)} = \frac{1 + a_1 z^{-1} + z^{-2}}{1 + ra_1 z^{-1} + r^2 z^{-2}} \quad (17)$$

where $a_1 = -2\cos(2\pi f_n t_s)$, $r \in [0,1]$, $x(k)$ is an input signal at a particular iteration k, $e(k)$ is the filter output signal at the same current iteration k, and t_s is a sampling time. To obtain a_1, the recursive maximum likelihood is implemented in the filter equation (17). Consequently, the main iterative loop is summarized as follows:

$$\varphi(k) = -x(k-1) + r(k)\,e(k-1) \quad (18)$$

where $e(k-1)$ is the output of the filter at the previous iteration, and φ_k is just an intermediate variable at the current iteration

$$\psi(k) = -\frac{\partial e(k)}{a_1} = \varphi(k)$$
$$- a_1(k-1)r(k)\psi(k-1) - r^2(k)\psi(k-2) \quad (19)$$
$$\bar{e}(k) = x(k) + x(k-2)$$
$$- r^2(k)\bar{e}(k-2) - \varphi^T(k)a_1(k-1) \quad (20)$$

where $\bar{e}(k)$ is *a priori* predicted output at the current iteration

$$p(k) = \frac{\left[\frac{p(k-1) - p(k-1)\psi(k)\psi^T(k)p(k-1)}{\lambda(k) + \psi^T(k)p(k-1)\psi(k)}\right]}{\lambda(k)} \quad (21)$$

where $p(k)$ is a gain factor, and $\lambda(k)$ is a forgetting factor which reduces the dependency of the updating process on the old samples.

$$a_1(k) = a_1(k-1) + p(k)\psi(k)\bar{e}(k) \quad (22)$$

where $a_1(k)$ is the estimated value at the current iteration

$$e(k) = x(k) + x(k-2) - r^2(k)e(k-2) - \varphi^T(k)a_1(k) \quad (23)$$

where $e(k)$ of (23) is a posteriori predicted output and is used in (18) in the next iteration

$$\lambda(k+1) = \lambda_o\lambda(k) + (1 - \lambda_o) \quad (24)$$
$$r(k+1) = r_0 r(k) + (1 - r_0)r_\infty. \quad (25)$$

Some parameters (a_1, p, ψ) are defined as ones, and some variables, such as $\lambda_o, \lambda(1), r(1), r_o$, are given as r_∞

$$r(1) = 0.8 \quad r_0 = 0.99 \quad r_\infty = 0.995$$
$$\lambda(1) = 0.95 \quad \lambda_0 = 0.99.$$

The iterative loop [(18)–(23)] is implemented to track the frequencies. Finally, the frequency of the flicker disturbance is obtained by

$$f_n = \frac{\cos^{-1}(-\frac{a_1}{2})}{2\pi t_s}. \quad (26)$$

APPENDIX B

The arc furnace model of [26] is listed as follows:

$$R_a = \begin{cases} R_g & 0 \le |i| < i_{ig} \\ \frac{V_d + (V_{ig} - V_d)e^{-(|i| - ig)/\tau_1}}{|i|} & |i| \ge i_{ig} \text{ and } \frac{d|i(t)|}{dt} \\ \frac{V_t + (V_{ig} - V_d)e^{-|i|/\tau_2}}{|i| + i_{ig}} & \frac{d|i(t)|}{dt} < 0 \end{cases}. \quad (27)$$

Given the following:

$$\begin{cases} V_{ig} = 1.15 V_d \\ i_{ig} = \frac{V_{ig}}{R_g} \\ \frac{V_t = \mathrm{I_{max}} + i_{ig}}{\mathrm{I_{max}}} \end{cases}. \quad (28)$$

The final arc resistance is given by

$$R_{arc}(t) = R_a(1 + m\sin(\omega_f t)).\qquad(29)$$

The parameters of the arc furnace model are

$$V_{ig} = 350.7 \text{ V}\quad V_t = 320.75 \text{ V}\quad R_g = 50 \text{ m}\Omega$$
$$I_{max} = 50 \text{ kA}\quad \tau_1 = 0.01\quad \tau_2 = 0.01$$
$$m = \text{random selection}\quad \omega_f = \text{random selection.}$$

APPENDIX C

This appendix gives some important parameters of the simulation and experimental setup.

For vector control- based simulation results:
- for PI in the q-ref. loop, $K_P = 1.25$, $K_I = 0.625$;
- for PI in V_{DC}, $K_P = 0.125$, $K_I = 0.0115$;
- for PI in the p-ref. loop, $K_P = 0.1$, $K_I = 0.05$;
- $V_{DC} = 10000$ V;
- hysteresis band = 5% of the maximum peak current.

For steepest decent-based simulation results:
- $\alpha = 0.05$;
- $M = 10$;
- $N = 400$.

For experimental results:
- the power switch is IRF 830;
- the hysteresis band = 10% of the maximum peak current;
- the sampling frequency for DSP = 6.4 kHz;
- L(filter) for the hysteresis circuit is 1.56 mH;
- C(filter) for the hysteresis circuit is 440 μF;
- $V_{DC} = 24$ V;
- program platform is eZdsp-LF2407A.

ACKNOWLEDGMENT

REFERENCES

[1] J. Schlabbach and D. Blume, "Voltage quality in electric power system," *Inst. Elect. Eng. Power Energy Ser.*, vol. 36, 2001.

[2] I. Vervenne, K. Van Reusel, and R. Belmans, "Electric arc furnace modeling from a power quality point of view," presented at the 9th Int. Conf. Elect. Power Qual. Utiliz., Barcelona, Spain, Oct. 9–11, 2007.

[3] O. Ozgun and A. Abur, "Flicker study using a novel arc furnace model," *IEEE Trans. Power Del.*, vol. 17, no. 4, pp. 1158–1163, Oct. 2002.

[4] D. Andrews, M. T. Bishop, and J. F. Witte, "Harmonic measurements, analysis, and power factor correction in a modern steel manufacturing facility," *IEEE Trans. Ind. Appl.*, vol. 32, no. 3, pp. 617–624, May/Jun. 1996.

[5] R. Collantes-Bellido and T. Gomez, "Identification and modeling of a three phase arc furnace for voltage disturbance simulation," *IEEE Trans. Power Del.*, vol. 12, no. 4, pp. 1812–1817, Oct. 1997.

[6] S. R. Mendis and D. A. Gonzalez, "Harmonic and transient over-voltage analyses in arc furnace power systems," *IEEE Trans. Ind. Appl.*, vol. 28, no. 2, pp. 336–342, Mar./Apr. 1992.

[7] T. Tayjasanant, W. Wang, C. Li, and W. Xu, "Interharmonic-flicker curves," *IEEE Trans. Power Del.*, vol. 20, no. 2, pt. 1, pp. 1017–1024, Apr. 2005.

[8] L. F. Beites, J. G. Mayordomo, A. Hernandez, and R. Asensi, "Harmonics, inter-harmonics and unbalance of arc furnaces a new frequency domain approach," *IEEE Trans. Power Del.*, vol. 16, no. 4, pp. 661–668, Oct. 2001.

[9] A. Elnady and M. M. A. Salama, "Unified approach for mitigating voltage sag and voltage flicker using the DSTATCOM," *IEEE Trans. Power Del.*, vol. 20, no. 2, pt. 1, pp. 992–1000, Apr. 2005.

[10] C. Han, Z. Yang, B. Chen, A. Q. Huang, B. Zhang, M. R. Ingram, and A.-A. Edris, "Evaluation of cascade-multilevel-converter-based STATCOM for arc furnace flicker mitigation," *IEEE Trans. Ind. Appl.*, vol. 43, no. 2, pp. 378–384, Mar./Apr. 2007.

[11] M. A. Hannan and A. Mohamed, "PSCAD/EMTDC simulation of unified series-shunt compensator for power quality improvement," *IEEE Trans. Power Del.*, vol. 20, no. 2, pt. 2, pp. 1650–1656, Apr. 2005.

[12] C. Schauder, "STATCOM for compensation of large electric arc furnace installations," presented at the IEEE Summer Meeting Power Eng. Soc., Edmonton, AB, Canada, 1999.

[13] G. F. Reed, J. E. Greaf, T. Matsumoto, Y. Yonehata, M. Takeda, T. Aritsuka, Y. Hamasaki, F. Ojima, A. P. Sidell, R. E. Chervus, and C. K. Nebecker, "Application of a 5 MVA, 4.16 kV D-STATCOM system for voltage flicker compensation at seattle iron and metals," presented at the IEEE Summer Meeting Power Eng. Soc., Chicago, IL, Jul. 2002.

[14] A. Elnady, "A single-phase current vector control for a DSTATCOM installed in distribution systems," presented at the IEEE Gulf Cooperation Council, Dubai, United Arab Emirates, 2011.

[15] T. Adali and S. Haykin, *Adaptive Signal Processing*. Hoboken, NJ: Wiley, 2010.

[16] Y. T. Chan and R. P. Langford, "Spectral estimation via the higher-order Yule-Walker equation," *IEEE Trans Acoust., Speech, Signal Process.*, vol. ASSP-30, no. 5, pp. 689–695, Oct. 1982.

[17] C. H. Haung, C. H. Lee, K. J. Shih, and Y. J. Wang, "Frequency estimation of distorted power system signals using a robust algorithm," *IEEE Trans. Power Del.*, vol. 23, no. 1, pp. 41–51, Jan. 2008.

[18] R. Aghazadeh, H. Lesani, M. Sanaye-Pasand, and B. Ganji, "New technique for frequency and amplitude estimation of power system signals," in *Proc. Inst. Elect. Eng., Gen., Transm., Distrib.*, May 2005, vol. 152, pp. 435–440.

[19] I. Y. H. Gu and M. H. J. Bollen, "Estimating interharmonics by using sliding-window ESPRIT," *IEEE Trans. Power Del.*, vol. 23, no. 1, pp. 13–23, Jan. 2008.

[20] B. Wirow and M. A. Lehr, "30 years of adaptive neural networks: Perceptron, madaline and backpropagation," *Proc. IEEE*, vol. 78, no. 9, pp. 1415–1445, Sep. 1990.

[21] P. Stoca and T. Solderstorm, "High-order Yule-Walker equation for estimating sinusoid frequencies: The complete set of solution," *J. Signal Process.*, vol. 20, no. 3, pp. 257–263, Jul. 1990.

[22] M. Mojiri, M. Karimi-Ghartemani, and A. Bakhshai, "Estimation of power system frequency using an adaptive notch filter," *IEEE Trans. Instrum. Meas.*, vol. 56, no. 6, pp. 2470–2477, Dec. 2007.

[23] M. Karimi-Ghartemani, M. R. Iravani, and A. R. Bakhashi, "A nonlinear adaptive notch filter for online signal analysis in power system applications," *IEEE Trans. Power Del.*, vol. 17, no. 2, pp. 617–622, Apr. 2002.

[24] S.-C. Pei and C.-C. Tseng, "Real-time adaptive notch filter scheme for sinusoidal parameter estimation," *J. Signal Process.*, pp. 117–130, 1994.

[25] Z. Hui, T. Wei, and Y. You-jun, "Simulations on harmonic analysis of arc furnace electrical arc model," in *Proc. 2nd Int. Conf. Inf. Eng. Comput. Sci.*, China, Dec. 25–26, 2010, pp. 1–4.

[26] T. Zheng and E. B. Makram, "An adaptive arc furnace model," *IEEE Trans. Power Del.*, vol. 15, no. 3, pp. 931–939, Jul. 2000.

[27] C. Schauder and H. Mehta, "Vector analysis and control of advanced static VAR compensators," in *Proc. Inst. Elect. Eng., Gen., Transm. Distrib.*, 1993, vol. 140.

[28] C. Schauder, M. Gernhardt, E. Stacy, T. Lemak, L. Gyugyi, T. W. Cease, and A. Edris, "Operation of ±100 MVA STATCON," *IEEE Trans. Power Del.*, vol. 12, no. 4, pp. 1805–1811, Nov. 1997.

[29] B. Singh, R. Saha, A. Chandra, and K. Al-Haddad, "Static synchronous compensators (STATCOM): A review," *Proc. Inst. Eng. Technol. Power Electron.*, vol. 2, no. 4, pp. 297–324, 2009.

[30] J. A. Pomilio and S. M. Deckmann, "Flicker produced by harmonic modulation," *IEEE Trans. Power Del.*, vol. 18, no. 2, pp. 387–392, Apr. 2003.

A. Elnady received the B.Sc. degree in electrical power and machines and the M.Sc. degree in power electronics applications from Cairo University, Cairo, Egypt, in 1994 and 1998, respectively, and the Ph.D. degree in power system operation and control from the University of Waterloo, Waterloo, ON, Canada, in 2004.

His research interests include power system control and operation, power-electronics applications in power and distribution systems, and digital-signal-processing applications in power systems.

Yan-Fei Liu (SM'09) received the B.Sc. and M.Sc. degrees in electrical engineering from Zhejiang University, Hangzhou, China, in 1984 and 1987, respectively, and the Ph.D. degree in electrical and computer engineering from Queen's University, Kingston, ON, Canada, in 1994.

From 1994 to 1999, he was a Technical Advisor with the Advanced Power System Division, Astec (formerly Nortel Networks), Ottawa, ON, Canada, where he was engaged in high-quality design, new products, and technology development. Since 1999, he has been with Queen's University, where he is currently a Professor in the Department of Electrical and Computer Engineering. His research interests include digital control technologies for dc–dc switching converters and ac–dc converters with power factor correction and current source, metal–oxide semiconductor field-effect transistor (MOSFET) drive technology, topologies and control for voltage regulator applications for dc–dc switching converters and ac–dc converters with power factor correction, current source MOSFET drive technology, topologies, and control for voltage regulator applications.

Dr. Liu has been an Associate Editor of IEEE TRANSACTIONS ON POWER ELECTRONICS since 2001. He is a Technical Program Chair for ECCE 2011. He is a Chair of the Technical Committee of Power Conversion Systems and Components of the IEEE Power Electronics Society. He was also Technical Program Chair for the 2010 International Workshop of Power Supply on Chip, Cork, Ireland, and Technical Program Vice Chair for ECCE 2010. He was a recipient of the 2001 Premiere's Research Excellent Award, Ontario, Canada, and the 1997 Award in Excellence in Technology from Nortel Networks.